ChemComm

COMMUNICATION

View Article Online
View Journal | View Issue

Cite this: *Chem. Commun.*, 2025, **61**, 8855

Received 31st March 2025,
Accepted 13th May 2025

DOI: 10.1039/d5cc01805f

rsc.li/chemcomm

Carbazole-functionalized Chichibabin diradicaloids with redshifted absorption and enhanced photoluminescence†

Vivek Chandrakant Wakchaure, [a] Xingmao Chang, [a] Julia Zolg, [bd] Rémi Blinder, [c] Mona E. Arnold, [b] Fedor Jelezko, *[cd] Alexander J. C. Kuehne *[bd] and Max von Delius *[ad]

Organic radicals and diradicaloids that are both stable and luminescent are promising candidates for molecular qubits in quantum technologies. Here we report two new carbazole-functionalized Chichibabin diradicaloids that in comparison to the parent compound TTM-TTM exhibit a 50 nm bathochromic shift of absorption and a 2–3-fold increase in PLQY.

Kinetically stabilized organic radicals are appealing objects of study due to their magnetic and optical properties.[1] Luminescent diradicaloids additionally have two distinct open-shell states (singlet and triplet).[2] Recently, substantial efforts have been dedicated to designing stable molecules with multiple π-conjugated radicals.[3] However, the development of organic radicals and diradicaloids that exhibit both bright luminescence and strong absorption in the near-infrared (NIR) region remains a challenge.[4]

Following our recent discovery of the **TTM-TTM**[5] diradicaloid (shortly after us also reported by Zhu *et al.* and Mesto *et al.*),[6] we wondered to what extent its absorption and emission bands are tuneable and its weak emission (PLQY 0.8%) can be enhanced. In this communication, we explore the impact of two- and four-fold carbazole donor substitution[7] on the optical and magnetic properties of Chichibabin-type diradicaloids (Fig. 1).

Starting from the known tris(2,4,6-trichlorophenyl)-methyl (**TTM**) radical, the iodinated precursor **Cbz$_2$-TTM-I** was obtained through a four-step sequence (Schemes S1 and S2, ESI†).[8] A statistical Ullmann coupling between **Cbz$_2$-TTM-I** and **TTM-I** delivered three products – one hetero-coupled and two homo-coupled compounds – in overall yield of 74% (Fig. 2a and Scheme S3, ESI†).[5] The isolation of all three diradicals **TTM-TTM** (24%), **Cbz$_2$-TTM-TTM** (**1**) (33%) and **Cbz$_2$-TTM-TTM-Cbz$_2$** (**2**) (17%) was possible by initial silica gel chromatography, as there is considerable difference in R_f values (Fig. S1, ESI†). The reference compound monoradical **Cbz$_2$-TTM-HTTM-Cbz$_2$** (**3**), was synthesized through Suzuki–Miyaura cross-coupling using **Cbz$_2$-TTM-I** and **Cbz$_2$-HTTM-Bpin** as starting materials (Scheme S4, ESI†).[9] The broad signal observed in the ^{1}H NMR spectrum suggests that the unpaired electron is not fully delocalized throughout the molecule (Fig. S49, ESI†). By contrast, both rigorously purified diradicals are completely NMR silent, highlighting their paramagnetic character (Fig. S43 and S45, ESI†).

Strict purification (after initial silica gel chromatography) is essential for investigating luminescent diradicaloids, because small amounts of the much brighter monoradicals, which are inevitably formed during Ullmann coupling (or during light exposure),[5] can lead to misleading results. To achieve exceptionally high purity, we painstakingly optimized both the

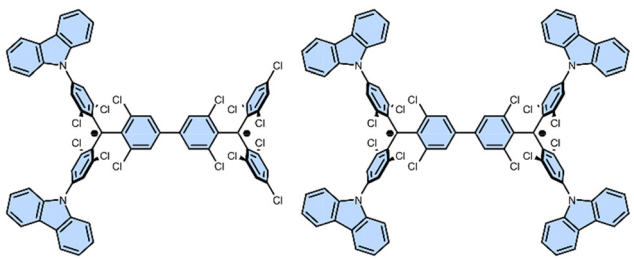

	1	**TTM-TTM**	**2**
λ_{max}(Abs)	640 nm	605 nm	663 nm
λ_{max}(PL)	825 nm	785 nm	827 nm
PLQY (%)	2.0	0.8	2.8

Fig. 1 Chemical structure of diradicaloids **1** and **2** with key properties *vs.* **TTM-TTM**[5] (gray box) (Abs: absorption; PL: photoluminescence; PLQY: photoluminescence quantum yield).

[a] *Institute of Organic Chemistry, Ulm University, Albert-Einstein-Allee 11, 89081 Ulm, Germany. E-mail: max.vondelius@uni-ulm.de*
[b] *Institute of Macromolecular and Organic Chemistry, Ulm University, Albert-Einstein-Allee 11, 89081 Ulm, Germany. E-mail: alexander.kuehne@uni-ulm.de*
[c] *Institute of Quantum Optics, Ulm University, Albert-Einstein-Allee 11, 89081 Ulm, Germany. E-mail: fedor.jelezko@uni-ulm.de*
[d] *Center for Integrated Quantum Science and Technology, Ulm University, Albert-Einstein-Allee 11, 89081 Ulm, Germany*

† Electronic supplementary information (ESI) available: Synthesis and characterization data, supplementary data on optical and magnetic properties. See DOI: https://doi.org/10.1039/d5cc01805f

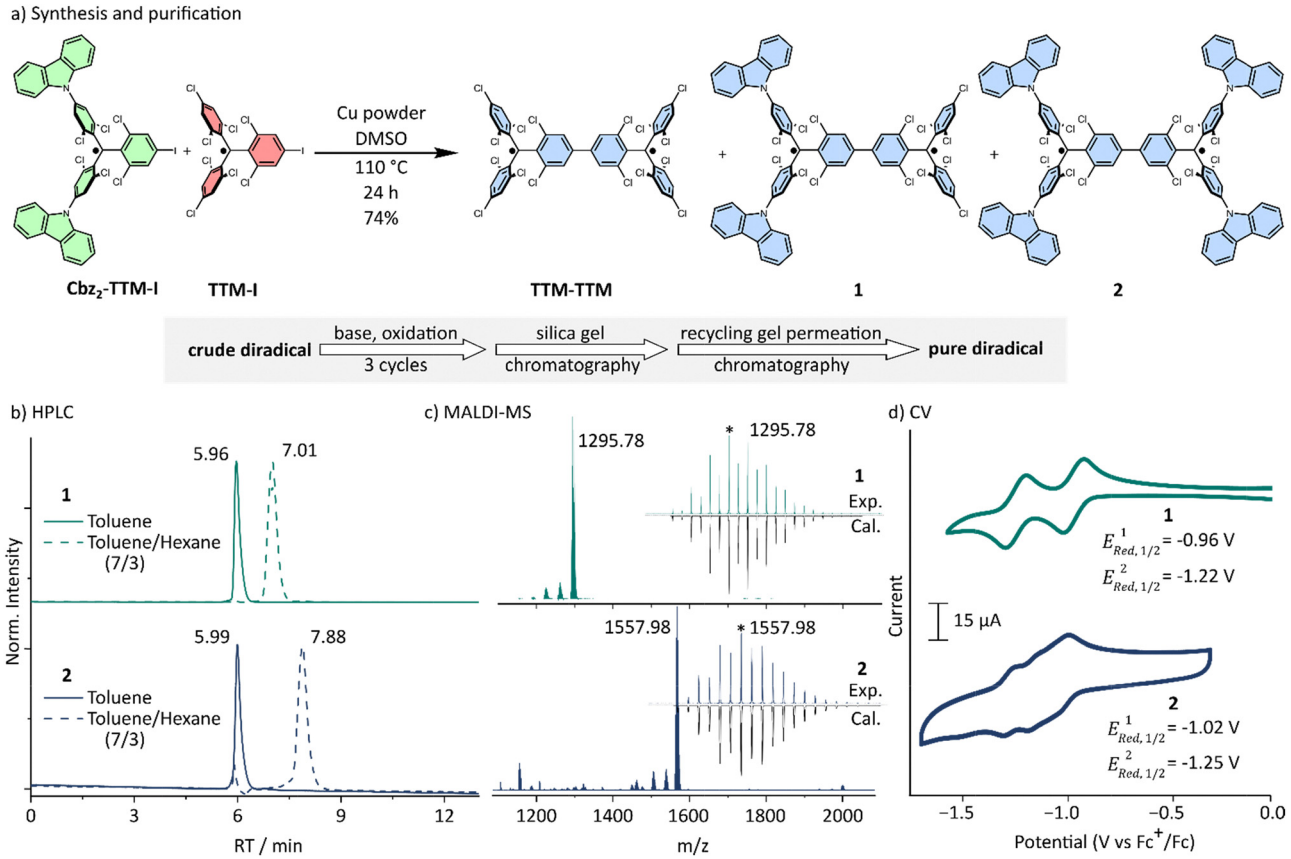

Fig. 2 (a) Statistical Ullmann synthesis of Chichibabin diradicaloids **TTM-TTM**, **1**, **2** and flow-chart of purification method. (b) Representative HPLC chromatograms (Buckyprep M, 0.5 mL min^{-1}). (c) High-resolution mass spectrometry (HR-MS, MALDI, positive mode) including isotopic patterns. (d) Cyclic voltammograms (CV) at a scan rate of 100 mV s^{-1} (glassy carbon (working), Pt wire (counter) and Ag/Ag^+ (reference) electrodes, 0.1 M $^nBu_4NPF_6$ in anhydrous CH_2Cl_2).

post-Ullmann chemical treatment and chromatographic purification methods. For instance, with a sample of **2**, we conducted multiple cycles of base treatment followed by oxidation and monitored the presence of **2** by UV-Vis spectroscopy after each cycle (Fig. S2, ESI†).

We observed that the intensity of the charge transfer (CT) band reached plateau after the 3rd base/oxidation cycle. The same treatment was applied to **1**. Following the base/oxidation cycles, products **1** and **2** were purified by silica gel chromatography (short plug) and recycling gel permeation chromatography (GPC) (Fig. S3–S6, ESI†). HR-MS (MALDI-TOF) proved to be a reliable indicator of compound purity, with significant deviations from the simulated isotopic patterns observed before purification (Fig. S4 and S6, ESI†), and excellent agreement achieved after purification (Fig. 2c and Fig. S44, S46, ESI†). High-performance liquid chromatography (HPLC, normal phase) corroborated the high chemical purity of all compounds (Fig. 2b and Fig. S7, S8 ESI†).

To shed light on the electrochemical properties, we conducted cyclic voltammetry (CV) experiments. The reference compounds **Cbz$_2$-TTM-I** and **3** show a single reversible oxidation at +0.45 V and +0.47 V, and reduction peaks at −0.98 V and −1.04 V, respectively, *versus* the ferrocenium/ferrocene (Fc^+/Fc) couple (Fig. S9 and S10, ESI†).[10] By contrast, the new diradicaloids undergo two reversible reduction processes, similar to the **TTM-TTM** molecule (Fig. 2d and Table 1 and Fig. S11 ESI†). Moreover, **1** shows two reversible oxidation peaks at +0.47 V and +0.89 V, which is similar to the parent compound **TTM-TTM**, whereas **2** shows broad reduction peaks due to its poor solubility and is unstable at high potential (Fig. S12, ESI†).[10b]

We proceeded with an investigation of photophysical properties. The UV-Vis absorption spectrum of the new diradicaloids in toluene solution exhibits a pronounced bathochromic shift (∼55 nm) upon substitution of **TTM-TTM** with two or four carbazole units, as shown in Fig. 3a.[6a] The reference monoradical

Table 1 Experimental and computational results on photophysical properties of the diradicaloids

Molecule	λ_{max} [nm] (Abs)	λ_{max} [nm] (PL)	ϕ [%]	ΔE_{ST}^{cal} [kcal mol^{-1}]	ΔE_{ST}^{exp} [kcal mol^{-1}]	t_{corr} [ns]	$\lvert D\rvert$ [MHz]	$E^1_{Red,1/2}$ [V]	$E^2_{Red,1/2}$ [V]
TTM-TTM[5]	605	785	0.8	−2.13	−3.11	16	231	−0.88	−1.18
1	640	825	2.0	−1.22	−1.60	31	246	−0.96	−1.22
2	663	827	2.8	−1.19	−1.32	54	437	−1.02	−1.25

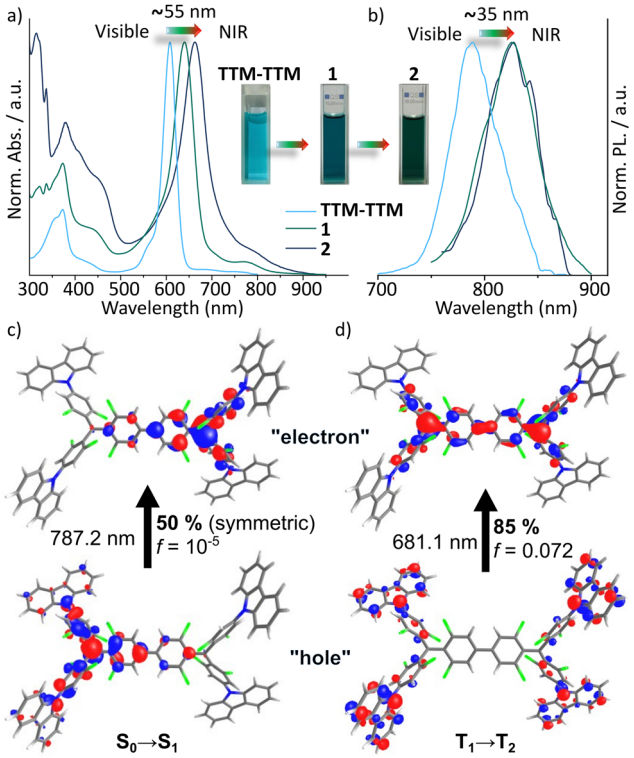

Fig. 3 (a) UV-Vis absorption spectra and photographs taken at ambient light. (b) Photoluminescence spectra in toluene solutions of **TTM-TTM**, **1**, and **2**. Natural transition orbitals (NTOs) with hole (h^+) and electron (e^-) for (c) the singlet and (d) the triplet state lowest energy transitions of **2** (in their optimized ground state geometry).

3 in contrast shows an absorption profile similar to its diradical counterpart (Fig. S13, ESI†), but the CT band at longer wavelengths is much weaker (Fig. S14–S16, ESI†).

Both diradicals exhibit broad emission bands in toluene, ranging from 750 to 900 nm with a λ_{max} of 825 nm, which is redshifted by approximately 35 nm compared to the parent compound, **TTM-TTM** (Fig. 3b). The PLQYs were determined to be 2.0% and 2.8% for **1** and **2**, respectively (Fig. S17, ESI†), representing an up to 3-fold enhancement compared to **TTM-TTM** (Table 1). This suggests that the incorporation of carbazole substituents significantly enhances the emission efficiency, albeit to a lesser extent than in the related monoradicals (Fig. S18, ESI†).[7b] The absorption maxima of both diradicals exhibit *ca.* 20 nm shift with increasing solvent polarity (Fig. S19, ESI†), indicating significant CT character. Time-dependent density functional theory (TD-DFT) calculations (Fig. S20–S28, ESI†) provide insights into the excited-state character of the diradicaloid systems. The natural transition orbitals (NTOs) of compound **2**, optimized in both singlet and triplet geometries, reveal distinct hole–electron localization. As shown in Fig. S29 (ESI†), the electronic structure can be described by resonance between open-shell diradical and closed-shell quinonoidal forms, with associated spin states and singlet–triplet energy gaps.[1g] The $S_0 \rightarrow S_1$ transition is dominated by a symmetry breaking charge separation, representing a dipole forbidden charge resonance state between the two radical centres in the molecule (see Fig. 3c, the $S_0 \rightarrow S_1$ transition is represented to 50% by the displayed NTO, the other 50% are represented by the exact mirror image). By contrast, the $T_1 \rightarrow T_2$ transition is represented (to 85%) by a CT with the hole residing on the donor carbazole units and the electron being delocalized over the **TTM-TTM** backbone (Fig. 3d). These results allow us to interpret the absorption in the visible spectrum of **2**. The small band at about 790 nm will originate from the $S_0 \rightarrow S_1$ transition, whereas the stronger absorption band at *ca.* 680 nm can be assigned to the $T_1 \rightarrow T_2$ transition. The calculated oscillator strengths (f) for these transitions also reflect the respective intensities (*cf.* Fig. 3a, c and d). The transitions for compound **1** can be assigned accordingly, however, here, the $S_0 \rightarrow S_1$ transition is dipole allowed due to the non-symmetrical structure of **1** (see NTOs in Fig. S24, ESI†). Moreover, the calculations indicated a singlet–triplet energy gap (ΔE_{ST}) of −1.22 and −1.19 kcal mol^{-1} for **1** and **2**, respectively (Table 1 and Tables S1–S4, ESI†), which agree well with experimental results (see below).

Turning our attention to magnetic properties, we found that reference monoradicals **Cbz$_2$-TTM-I** and **3** exhibit nearly identical electron paramagnetic resonance (EPR) spectra in toluene at room temperature (Fig. 4a and Fig. S30, ESI†). At 190 K in liquid toluene, both diradicaloids **1** and **2** display a sharp central peak, accompanied by two broad shoulders in their EPR spectra. The two broad shoulders correspond to the dominant diradical species, as shown in the inset of Fig. 4a. We successfully simulated the data with the diradical species modelled as a spin-triplet state characterized by a zero-field splitting parameter ($|D|$) (Fig. S31, S32 and Tables S5, S6 ESI†). The fitted values of $|D|$ are 246 MHz for **1** and 437 MHz for **2**, reflecting the strength of the dipolar interaction within the radical pair.[11] Notably, these values both exceed that of the parent derivative **TTM-TTM** (231 MHz),[5] indicating that the presence of the donor moiety influences the dipolar interaction within the radical pair, likely through modifications in the electronic structure and spatial

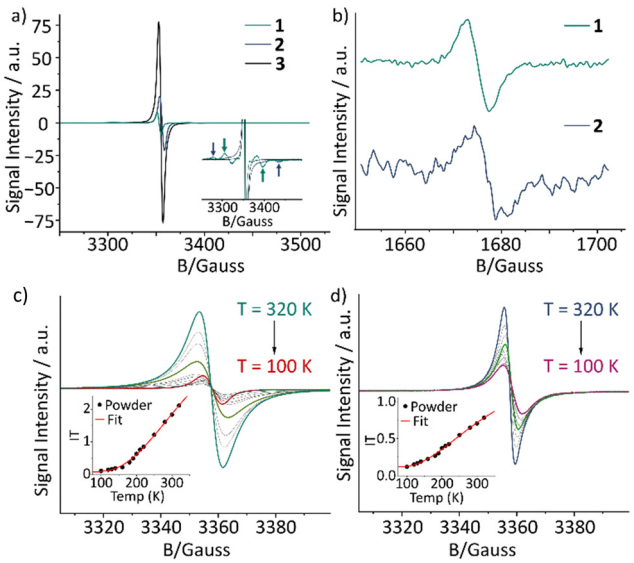

Fig. 4 (a) EPR spectra of **1**, **2** and **3** in toluene at 190 K, inset: normalised zoom spectra, the arrows indicate the shoulders related to the diradical species. (b) Half-field transitions of the **1** and **2** in toluene at 170 K. VT-EPR spectra of powder samples (c) **1**, (d) **2** from 320 to 100 K. Insets: The solid lines are the fitting curves according to the Bleaney–Bowers equation.

distribution of the unpaired spins. Moreover, a rotational correlation time (t_{corr}) of 16 ns, 31 ns, and 54 ns (at 190 K in toluene) for **TTM-TTM**, **1**, and **2**, respectively, is consistent with the expected variation (increase) in the molecular hydrodynamic radius upon the addition of carbazole units. Additionally, the observation of the forbidden $\Delta m_s = \pm 2$ transition (half-field) confirms the diradical character, as this transition is specific to triplet-state species exhibiting substantial spin–spin interactions (Fig. 4b). The variable-temperature (VT) EPR measurements (320–100 K) in powder show that the spectral intensity decreases with decreasing temperature, suggesting a singlet open-shell ground state as previously also observed for the parent compound **TTM-TTM** (Fig. 4c and d).[5] The ΔE_{ST} was estimated by fitting the EPR curves using the Bleaney–Bowers equation.[12] The values obtained were −1.60 and −1.32 kcal mol^{-1} for **1** and **2**, respectively, which are lower than that of **TTM-TTM** (−3.11 kcal mol^{-1}), these values are in excellent agreement with the DFT calculations (Table 1).

In conclusion, our findings demonstrate that the magnetic and optical properties of kinetically stabilized trityl diradicaloids are tunable by carbazole substitution. These insights will guide future work from diradicaloids to polyradicaloids.[13]

X. C. thanks the Alexander von Humboldt Foundation for a postdoctoral fellowship and Ulm University for a start-up funding for junior researchers (P9854051). We acknowledge financial support by the German Research Foundation (DFG, 445471845, 445471097 and 445470598, 364549901 SFB TRR 234 "CataLight" (project B7)) and the German Federal Ministry of Education and Research (BMBF, project QuE-MRT). The authors acknowledge support by the state of Baden-Württemberg through bwHPC and the DFG through grant no INST 40/575-1 FUGG (JUSTUS 2 cluster). This work was carried out within the framework of the Center for Integrated Quantum Science and Technology (IQST). J. Z. acknowledges IQST for a PhD program within the IQST Graduate School@-Quantum^{BW} supported by the Baden-Württemberg Ministry of Science, Research, and Arts. F. J. group was funded by the German Federal Ministry of Research (BMBF) by future cluster QSENS, Deutsche Forschungsgemeinschaft (DFG), and Carl-Zeiss-Stiftung *via* the Center of Integrated Quantum Science and technology (IQST) and project Ultrasens-Vir.

Data availability

The data supporting this article have been included as part of the ESI† and coordinates of the geometry optimized structures are openly available *via* Zenodo under **https://doi.org/10.5281/zenodo.15363783**.

Conflicts of interest

There are no conflicts to declare.

References

1 (*a*) Z. X. Chen, Y. Li and F. Huang, *Chem*, 2021, **7**, 288–332; (*b*) S. V. S. Sowndarya, P. C. St John and R. S. Paton, *Chem. Sci.*, 2021, **12**, 13158–13166; (*c*) A. Mizuno, R. Matsuoka, T. Mibu and T. Kusamoto, *Chem. Rev.*, 2024, **124**, 1034–1121; (*d*) P. Murto and H. Bronstein, *J. Mater. Chem. C*, 2022, **10**, 7368–7403; (*e*) Z. Zeng, X. Shi, C. Chi, J. T. L. Navarrete, J. Casado and J. Wu, *Chem. Soc. Rev.*, 2015, **44**, 6578–6596; (*f*) I. Ratera and J. Veciana, *Chem. Soc. Rev.*, 2012, **41**, 303–349; (*g*) J. J. Dressler and M. M. Haley, *J. Phys. Org. Chem.*, 2020, **33**, e4114.

2 (*a*) K. Günther, N. Grabicki, B. Battistella, L. Grubert and O. Dumele, *J. Am. Chem. Soc.*, 2022, **144**, 8707–8716; (*b*) Y. Hattori, E. Michail, A. Schmiedel, M. Moos, M. Holzapfel, I. Krummenacher, H. Braunschweig, U. Müller, J. Pflaum and C. Lambert, *Chem. – Eur. J.*, 2019, **25**, 15463–15471; (*c*) Y. R. Poh and J. Y. Zhou, *ACS Cent. Sci.*, 2025, **11**, 116–126; (*d*) P. Ravat, T. Šolomek, M. Rickhaus, D. Häussinger, M. Neuburger, M. Baumgarten and M. Juríček, *Angew. Chem., Int. Ed.*, 2016, **55**, 1183–1186; (*e*) L. Valenta, M. Mayländer, P. Kappeler, O. Blacque, T. Šolomek, S. Richert and M. Juríček, *Chem. Commun.*, 2022, **58**, 3019–3022.

3 (*a*) S. M. Kopp, S. Nakamura, B. T. Phelan, Y. R. Poh, S. B. Tyndall, P. J. Brown, Y. Huang, J. Y. Zhou, M. D. Krzyaniak and M. R. Wasielewski, *J. Am. Chem. Soc.*, 2024, **146**, 27935–27945; (*b*) A. Mizuno, R. Matsuoka, S. Kimura, K. Ochiai and T. Kusamoto, *J. Am. Chem. Soc.*, 2024, **146**, 18470–18483; (*c*) R. Matsuoka, S. Kimura, T. Miura, T. Ikoma and T. Kusamoto, *J. Am. Chem. Soc.*, 2023, **145**, 13615–13622; (*d*) A. Abdurahman, J. Wang, Y. Zhao, P. Li, L. Shen and Q. Peng, *Angew. Chem., Int. Ed.*, 2023, **62**, e202300772; (*e*) P. Bartos, D. Pomikło, K. B. Sorenson, O. Hietsoi, A. C. Friedli and P. Kaszyński, *J. Am. Chem. Soc.*, 2025, **147**, 125–129.

4 (*a*) Y. Zhu, Z. Zhu, S. Wang, Q. Peng and A. Abdurahman, *Angew. Chem., Int. Ed.*, 2025, **64**, e202423470; (*b*) D. Zhang, Z. Zhu, X. Xiao, Y.-H. Fang, T. Xiao, X. Wang, S.-D. Jiang and D. Zhao, *J. Am. Chem. Soc.*, 2024, **146**, 21752–21761; (*c*) C. Yan, D. An, W. Chen, N. Zhang, Y. Qiao, J. Fang, X. Lu, G. Zhou and Y. Liu, *CCS Chem.*, 2022, **4**, 3190–3203; (*d*) Q. Peng, A. Obolda, M. Zhang and F. Li, *Angew. Chem., Int. Ed.*, 2015, **54**, 7091–7095; (*e*) P. Murto, R. Chowdhury, S. Gorgon, E. Guo, W. Zeng, B. Li, Y. Sun, H. Francis, R. H. Friend and H. Bronstein, *Nat. Commun.*, 2023, **14**, 4147; (*f*) M. E. Arnold and A. J. C. Kuehne, *Dyes Pigm.*, 2023, **208**, 110863; (*g*) X. Ai, E. W. Evans, S. Dong, A. J. Gillett, H. Guo, Y. Chen, T. J. H. Hele, R. H. Friend and F. Li, *Nature*, 2018, **563**, 536–540; (*h*) A. Borissov, P. J. Chmielewski, C. J. Gómez García, T. Lis and M. Stępień, *Angew. Chem., Int. Ed.*, 2023, **62**, e202309238.

5 X. Chang, M. E. Arnold, R. Blinder, J. Zolg, J. Wischnat, J. van Slageren, F. Jelezko, A. J. C. Kuehne and M. von Delius, *Angew. Chem., Int. Ed.*, 2024, **63**, e202404853.

6 (*a*) Z. Zhu, Z. Kuang, L. Shen, S. Wang, X. Ai, A. Abdurahman and Q. Peng, *Angew. Chem., Int. Ed.*, 2024, **63**, e202410552; (*b*) D. Mesto, M. Orza, B. Bardi, A. Punzi, I. Ratera, J. Veciana, G. Farinola, A. Painelli, F. Terenziani, D. Blasi and F. Negri, *Chem. – Eur. J.*, 2025, e202500749.

7 (*a*) M. E. Arnold, L. Roß, P. Thielert, F. Bartley, J. Zolg, F. Bartsch, L. A. Kibler, S. Richert, C. Bannwarth and A. J. C. Kuehne, *Adv. Opt. Mater.*, 2024, **12**, 2400697; (*b*) S. Castellanos, D. Velasco, F. López-Calahorra, E. Brillas and L. Julia, *J. Org. Chem.*, 2008, **73**, 3759–3767; (*c*) L. Fajarí, R. Papoular, M. Reig, E. Brillas, J. L. Jorda, O. Vallcorba, J. Rius, D. Velasco and L. Juliá, *J. Org. Chem.*, 2014, **79**, 1771–1777; (*d*) S. Kasemthaveechok, L. Abella, M. Jean, M. Cordier, T. Roisnel, N. Vanthuyne, T. Guizouarn, O. Cador, J. Autschbach, J. Crassous and L. Favereau, *J. Am. Chem. Soc.*, 2020, **142**, 20409–20418; (*e*) K. Matsuda, R. Xiaotian, K. Nakamura, M. Furukori, T. Hosokai, K. Anraku, K. Nakao and K. Albrecht, *Chem. Commun.*, 2022, **58**, 13443–13446.

8 (*a*) O. Armet, J. Veciana, C. Rovira, J. Riera, J. Castaner, E. Molins, J. Rius, C. Miravitlles, S. Olivella and J. Brichfeus, *J. Phys. Chem.*, 1987, **91**, 5608–5616; (*b*) G. Battagliarin, C. Li, V. Enkelmann and K. Müllen, *Org. Lett.*, 2011, **13**, 3012–3015.

9 Z. Li, J. Wang, X. Liu, P. Gao, G. Li, G. He and B. Rao, *Angew. Chem., Int. Ed.*, 2023, **62**, e202302835.

10 (*a*) V. S. Mothika, M. Baumgarten and U. Scherf, *ACS Appl. Nano Mater.*, 2019, **2**, 4832–4841; (*b*) S. H. Hsiao and S. W. Lin, *Polym. Chem.*, 2016, **7**, 198–211.

11 G. Jeschke, *Macromol. Rapid Commun.*, 2002, **23**, 227–246.

12 B. Bleaney, *Rev. Mod. Phys.*, 1953, **25**, 161–162.

13 T. Y. Gopalakrishna, W. Zeng, X. Lua and J. Wu, *Chem. Commun.*, 2018, **54**, 2186–2199.

